

**IMECE2018-87897**

## **Porosity Analysis in Metal Additive Manufacturing by Micro-CT**

**Subin Shrestha, Thomas Starr, Kevin Chou**

Additive Manufacturing Research Center  
University of Louisville  
Louisville, KY, 40292, USA

### **KEYWORDS**

Microcomputed Tomography; Selective Laser Melting; Pore Characterization

### **ABSTRACT**

This study aims at analyzing process-induced pores in selective laser melting (SLM), a laser powder-bed fusion additive manufacturing (AM) process. Porosity is one of the most problematic defects in SLM parts; it impairs the part performance, and yet, is sharply sensitive to the parameters of the SLM process itself. Detailed analysis of SLM pore formations using a computed tomography (CT) technique is desired in order to understand the porosity level at different process conditions. In this study, an SLM system was used to fabricate samples, using Ti-6Al-4V powder, with single tracks formed, at 60  $\mu\text{m}$  layer thickness, with different laser powers and scanning speeds to vary the energy density. A micro-CT ( $\mu\text{-CT}$ ) scanner was used to measure the internal features of the SLM specimens without any post-build treatments and to analyze the porosity inside single tracks formed with different energy densities. There are different mechanisms of pore formation in SLM, in particular, this study first focuses on the pore formation due to the keyhole phenomenon, caused by a high energy density.  $\mu\text{-CT}$  scanning at a 6  $\mu\text{m}$  resolution is able to clearly reveal the pores in the SLM samples. From the CT scan and analysis results, it is observed that increasing the energy density increases the volume of pores. For example, with 195 W and 200 mm/s, the number of pores is 93 and the total pore volume is 0.014  $\text{mm}^3$  for a scanning length of 12 mm. On the other hand, if the energy density is less than 0.24 J/mm, few or no pores were

observed, because possibly the melting process changes from the keyhole mode to the conduction mode.

### **INTRODUCTION**

Selective laser melting (SLM) is a powder bed additive manufacturing (AM) process in which parts are fabricated by continuous scanning of powder layer based on computer aided design (CAD) data. Thus fabricated part quality depend upon various process parameters such as laser power, scanning speed, scanning strategy, layer thickness, energy distribution etc. [1]. It is always desired to optimize part for which a single track formation can be studied at different energy densities [2]. Energy density, which is the function of laser power, scanning speed, layer thickness and hatch spacing would determine the mode of melting during SLM process. Rai et. al. [3] have demonstrated in laser welding process that, when laser power and speed exceeds certain criteria, the mode changes from conduction to keyhole-mode at which significant pores would form. In similar manner, pore in SLM process can be formed due to partial melting [4] or keyhole mode laser melting [5]. Lack of fusion porosity has higher effect on part strength even if present in small volume percentage compared to the keyhole pores which appear to be harmless [6]. In addition, pores are undesirable in the sense that they have negative effect on the fatigue behavior of SLM parts [7]: pore count and their location are critical to the stress concentration. As the pore diminishes mechanical strength of the SLM parts, it is desired to reduce pores which may form due to keyhole mode laser melting at very high energy density or partial melting due to very low energy density. Laser power and

scanning speed which contributes to energy density should be properly selected in order to have least porosity possible.

Few studies have been carried out to investigate the formation of pores at different energy densities. Gong et al. [8] studied the effect of different energy density in the formation of melt pool boundary and keyhole pores were observed at high energy density. Aboulkhair et al. [9] investigated the effect of different process parameters such as laser power, scanning speed, hatch spacing, etc. to find the windows of parameters required to produce high density parts from AlSi10Mg. The metallographic study showed that there may be formation of metallurgical or keyhole pores depending on the process parameter selected. Besides, with AlSi10Mg, hydrogen porosity may form due to the presence of moisture in powder particle surface as well as dissolved hydrogen in the powder material [10]. These hydrogen porosity are however observed in aluminum processing only and are not present in other material processing. Ponnusamy et al. [11] performed statistical analysis of porosity of 17-4PH stainless steel considering different process parameters such as laser power, defocus distance, layer thickness and build orientation which also helped to find optimum process parameters. Although, metallographic study clearly shows the pores at different energy density levels, it does not provide complete information regarding pores.

King et al. [5] explained the observation of keyhole mode laser melting during SLM process. As the energy density is reduced, the keyhole mode laser melting transforms to conduction mode melting. Moreover, the keyhole pores are formed due to the collapse of vapor cavity as a result of evaporation of metal. The characterization of pore formed due to keyhole melting as well as partial melting would help achieve better process parameters. Since, pores may be formed in random manner, it is desired to have a complete study of internal structure of SLM parts and microcomputed tomography ( $\mu$ CT) has been established to study internal features of desired part. However, SLM process deals with high density metals which would complicate the scanning procedure. Nevertheless, it has been shown that  $\mu$ CT can be used to examine the void morphology along the scan tracks formed by SLM of 316L stainless steel [5]. In addition,  $\mu$ CT has been applied to study the interior voids formed during SLM of aluminum alloy[12], cobalt-chrome[13], Ti-6Al-4V [14].

In this study, single tracks with different energy densities are formed on top of previously build surface by changing laser power and scanning speed. These single tracks are formed inside the hollow powder container which is designed with features to assist in  $\mu$ CT scanning. Pore count and pore volume are obtained for different energy density along with detailed pore morphology study.

## METHOD

### SLM specimen fabrications

EOS M270 was used to fabricate SLM specimens for porosity analysis in this study. Ti-6Al-4V powder particles with the size below 45  $\mu$ m were used and the layer thickness for the single track is 60  $\mu$ m. To systematically and consistently access the build regions subject to CT measurements, a small cylinder-shape model of half-solid and half-hollow was designed. Figure

1 (a) shows the CAD model of a semi-hollow cylinder. The notches with end-to-end dimension of 12 mm were included to identify the start and end of single tracks. Within one specimen, four single tracks were formed, with specified process parameters, at the top of the base pad (half-solid cylinder). The specimens of such a model were then fabricated in M270; Figure 1(b) shows the specimens after the build completion. Design of experiment was developed with 4 power level (125W, 150W, 175W and 195W) and 6 scanning speeds (200 mm/s, 400 mm/s, 600 mm/s, 800 mm/s, 1000 mm/s and 1200 mm/s) which resulted in 24 single track with different process parameters. Therefore 6 samples were designed to include those single tracks.

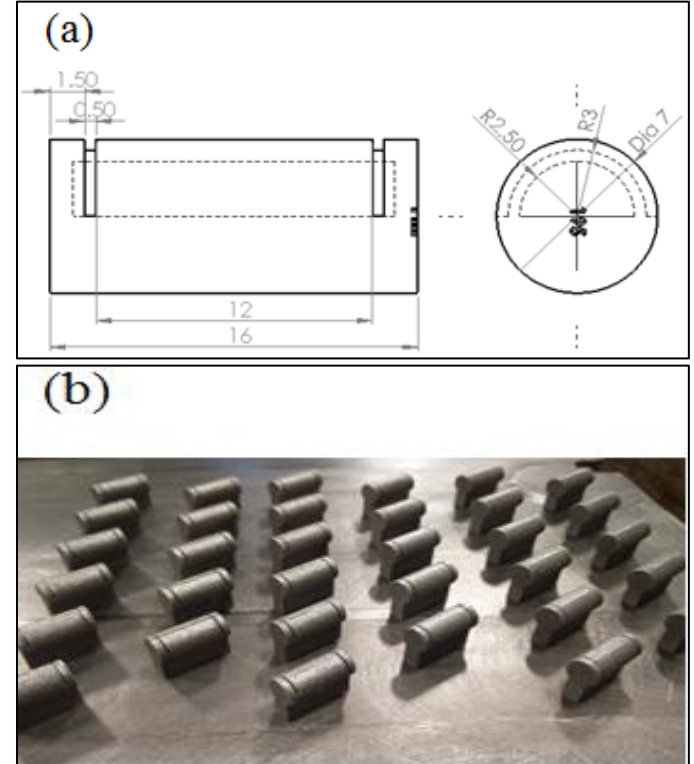


Figure 1: (a) CAD model of the specimen (unit in mm) and (b) Semi-hollow cylinders with single track built on the base plate.

### CT scanning

CT scanning of the fabricated single-track SLM specimens was performed in a Bruker SkyScan 1173 micro-CT scanner shown in Figure 2(a). The test specimens were positioned in the brass sample mount using clay, styrofoam and parafilm tape as shown in Figure 2 (c). Styrofoam and parafilm tape being radiotransparent do not affect the scanning of highly dense Ti-6Al-4V. A magnification of 6  $\mu$ m was used and samples were scanned at 2000 pixel resolution. 130 kV x-ray source with 8 W power was generated which is filtered through a 0.25 mm brass filter so as to absorb x-ray with energy below 60 kV. This is necessary for highly dense materials to reduce beam hardening artifact otherwise the outer surface would appear more dense than interior due to higher absorption of low energy x-rays near outer surface. Each scan took about 17.5 hours while using 0.1° rotational angle to perform complete 360° scanning. Due to long scanning time, flat field correction was performed every 60

minutes to minimize the effect of thermal movement. As a result, the reconstruction process did not require project pixel shift corrections. After scanning was completed, the steps towards reconstruction were followed. Beam hardening of 30% have been used which remained the same for all the samples. Ring artifacts and misalignment compensations were performed using parameter fine-tuning to minimize the ring artifacts and blurring effects, etc.

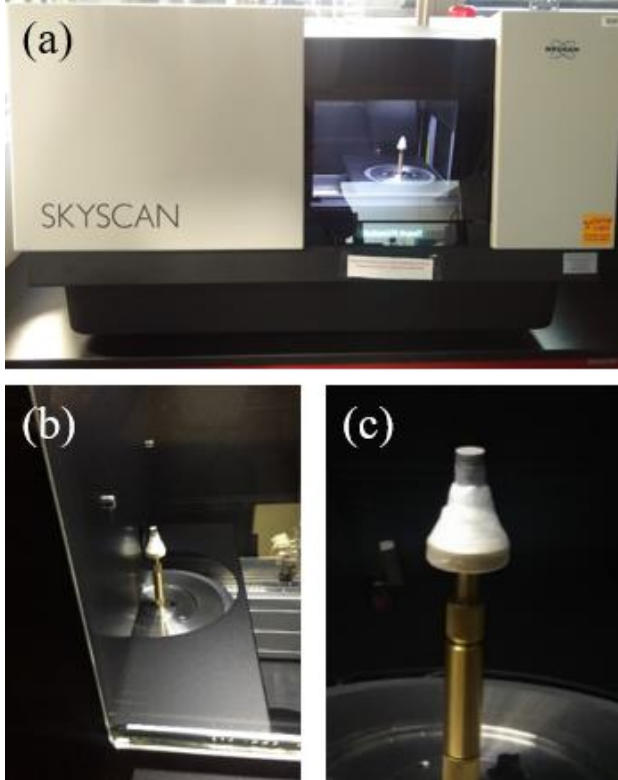


Figure 2: (a) Skyscan 1173 micro-CT scanner, (b) Specimen setup in the CT system showing near x-ray window, and (c) closed-up view of sample mounting.

CTan software was then used to analyze the reconstructed data which is series of Z-cross section images with  $6 \mu\text{m}$  difference between successive image slices. At first, top and bottom for the volume of interest were selected which defined the start and end of scanning track. Then, a rectangular region of interest (ROI) was specified which was kept consistent for every track in all specimens. The region of  $0.4 \text{ mm} \times 0.5 \text{ mm}$  was selected and the position was changed based on the slice to exclude the powder area from the region of interest. Figure 3 below illustrates the region of the interest in reference to one single track. After the ROI was expanded to all slices, the binary images were obtained. Then, 3D morphometry analysis was performed to obtain the pore information such as pore number, individual pore volume etc. Since the number of pores from each single track was limited, individual pore analysis has been conducted. The individual pore analysis help obtain the pore volume of any specific pore along with its location along the single track.

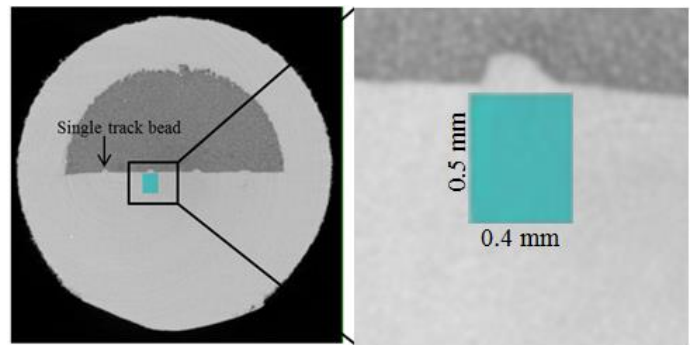


Figure 3: Selection of ROI beneath single track for porosity analysis.

## RESULTS AND DISCUSSION

### Typical scanning images

Figure 4 shows example of CT images from a typical specimen with different sectional views as well as the isometric partial cutoff view. The color coding is based on the density of the material: light grey area is solid, medium grey area is powder and the dark spots in the sagittal view, with represent density of air, are pores. Four single tracks formed atop of base pad are clearly identified. These four tracks, in the figure shown are formed with 195 W laser power and 200 mm/s, 400 mm/s, 600 mm/s and 800 mm/s scanning speed (from right to left). When a cross section is taken somewhere in the middle of 200 mm/s single track numerous voids can be observed. These are the pores due to keyhole formation when the recoil pressure creates huge depression which was not filled before the solidification and the void were entrapped. In addition, Figure 5 shows the binary image of a pore at successive slices and the rendered 3D representation of a pore from the 2D information. 3D view of pores was generated using CTvox software by density cutoff which removes the highly dense Ti-6Al-4V solid from the view. With this, the shape distribution of pores at different energy densities can be investigated.

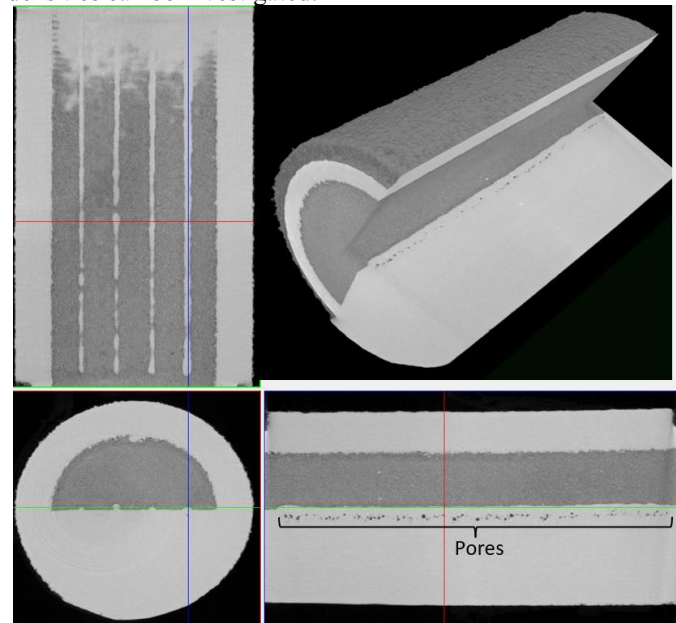


Figure 4: Examples of CT images of a scanned SLM specimen.

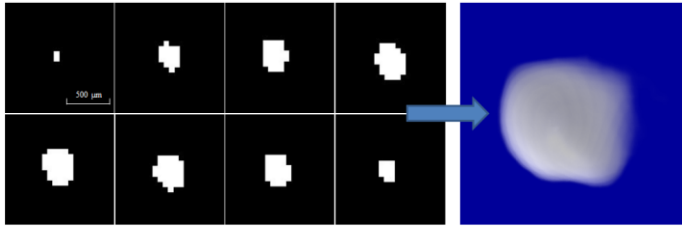


Figure 5: 3D rendering of a pore from 2D binary images.

#### Single track morphology

CT scanning result can also be analyzed to obtain the single track morphology. Figure 6 depicts the single track morphology obtained from 195W 200-800 mm/s sample. This was achieved by changing the transfer function in CTVox which allowed discarding the low density powder from the view and only looking at the higher density single track formed on top of base pad. This procedure was applied for each sample and morphology at each combination was investigated. Figure 8 shows the single track morphology at different power and speed combination. With this study, we can separate dense single track with partially melted single track. Tracks with partial melting would not result in good build surface and therefore would not be considered for further studies.

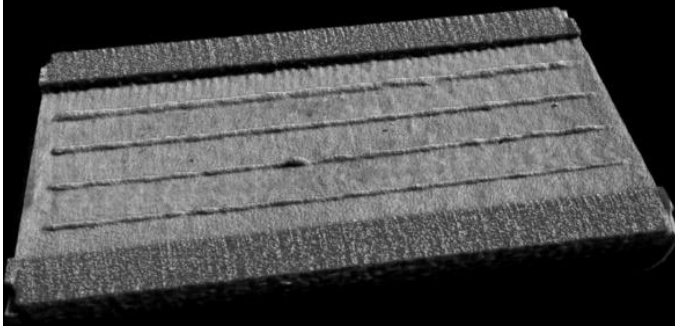


Figure 6. Single track morphology obtained from one sample.

We observe from Figure 7 that the density of single track is function of speed as well as power. Furthermore, track width is also the function of energy density, and for same power, track width decreased with increasing scanning speed. Although for 195 W power all the single track looks dense, interior pore should also be studied prior to confirming that an specific process parameter is better. However, for 125 W, the balling behavior begins to appear at speed above 1000 mm/s. These tracks are not dense enough and would probably result in very rough surface or porous surface during area scanning.

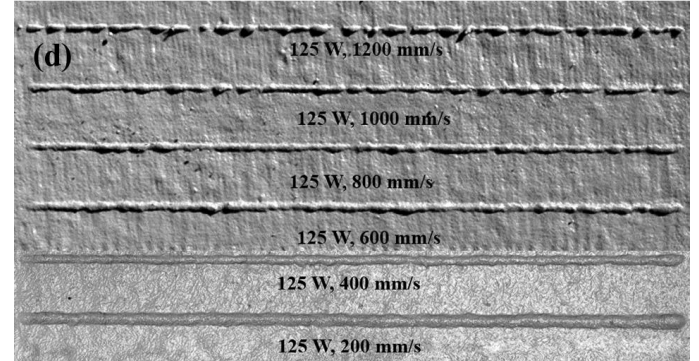
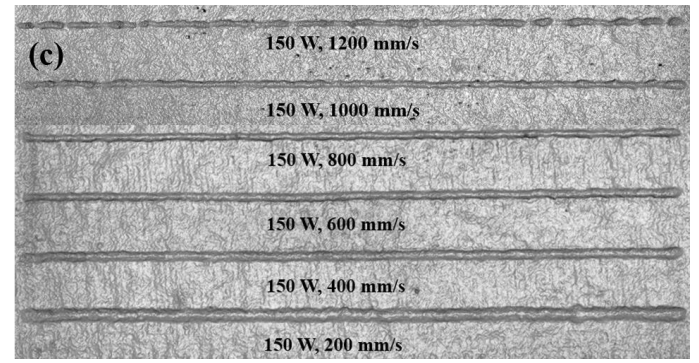
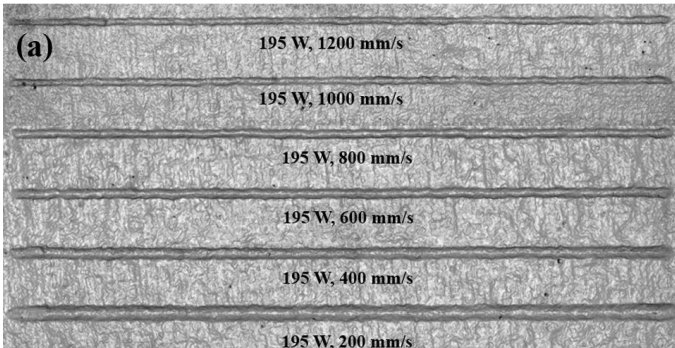


Figure 7. Single track morphology at different scanning speeds when power is (a) 195 W, (b) 175 W, (c) 150 W and (d) 125 W.

#### Pore characteristics

To quantitatively characterize porosity, pore counts and individual volumes were obtained from CTan. For example, for 195 W power and 200 mm/s scanning speed, which has the maximum energy density (0.975 J/mm), the specimen exhibits 93 pores over the scanning length of 12 mm. On the other hand, for the specimen with 195 W and 400 mm/s, total 50 pores were formed. Figure 8 shows the morphology and volume of each pore along the scanning direction for later case. We may observe huge variation in pore volume which may be due to the instability during the formation of melt pool as a result of keyhole effect.

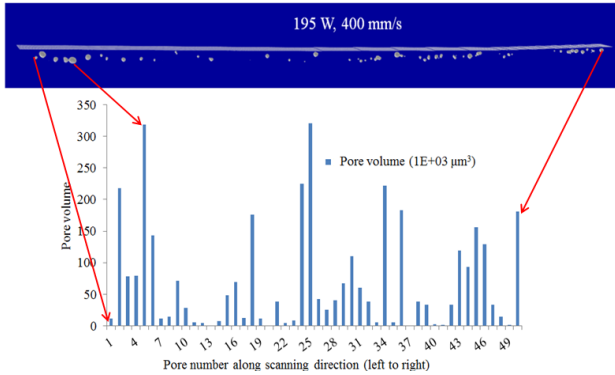


Figure 8: Pore volume along the scanning track of 195 W, 400 mm/s case.

Sphericity ( $\psi$ ), is a measure of how close a body is to the mathematically perfect sphere which can be calculated by using the relationship

$$\psi = \frac{\pi^{\frac{1}{3}} (6V_p)^{\frac{2}{3}}}{A_p}$$

Where  $V_p$  is the volume of the object and  $A_p$  is the surface area

Sphericity can be used characterize and differentiate between pores formed due to low energy density and high energy density [15]. The sphericity of all the pores were above 0.7 which indicates that the pores are result of keyhole mode melting. Among 50 pores, first 9 pore details have been mentioned in this paper: the location of pores were identified with respect to the beginning of single track and free surface on which single tracks are formed. Table 1 lists the position and property of 9 pores whose centroid are located within 1.5 mm of initial scan length. Due to higher penetration, pores are formed at depth of above 130  $\mu\text{m}$ . Such amount of penetration is undesirable and must be eliminated to ensure no keyhole pores are formed during the part fabrication.

Table 1: Pore characteristics

Pore no.	Volume ( $\mu\text{m}^3$ )	Sphericity	Major diameter ( $\mu\text{m}$ )	Distance from initial scan vector	Depth from free surface
1	167777.01	0.91	79.51	114	145.90
2	318.00	0.84	14.67	366	161.36
3	10559.72	0.88	33.62	366	169.09
4	29331.52	0.92	45.93	528	138.17
5	121329.21	0.89	74.29	666	174.90
6	146657.58	0.89	83.19	864	153.63
7	85113.77	0.90	68.65	984	154.60
8	105223.07	0.83	96.42	1086	170.06
9	29350.22	0.90	46.40	1320	138.17

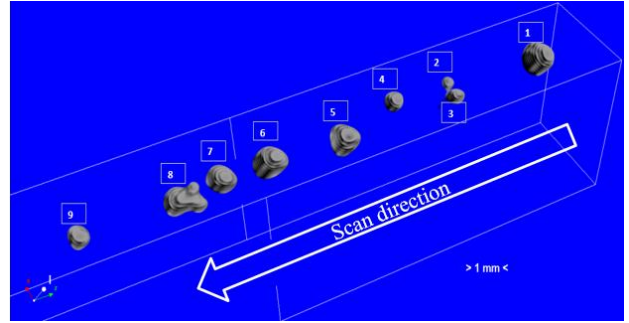


Figure 9: Detail view of pore morphology.

#### Process parameter effects

The energy density during laser scanning, directly related to the laser power and scanning speed plays a critical role of the keyhole phenomenon and associated pore formations. When the laser power is kept constant, decreasing the scanning speed increases the energy density, and therefore, promotes the formation of keyhole pores. As an example, Figure 10 compares between different speeds when the laser power is 195W. We may notice that for 200 mm/s scanning speed, a series of pores are formed which are well below the solid-powder interface. The keyhole effect is less noticeable for 600 mm/s, whereas the pore numbers decrease significantly for 1000 mm/s at which the energy density may be below threshold of keyhole mode melting. Figure 11 shows the rendered 3D pore morphology observed at different scanning speed for 195 W laser power. At 1000 mm/s, only one pore is noticed which was formed at the end of the scan track. At the laser turn off spot, the solidification rate is higher and melt flow is not significant. As a result, if the depression formed during melting is higher, there is a chance that pores would be formed at the end of the scan track. Keyhole pores in SLM process did not have an obvious shape transformation with respect to energy density as that in laser welding process [16], however pore volume and pore count significantly varied among different energy densities.

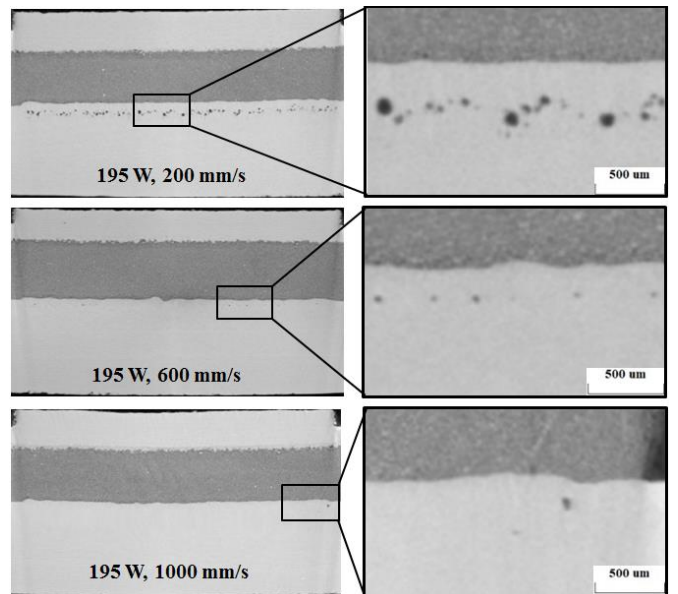


Figure 10: 2D images for pore comparisons between different scanning speeds.

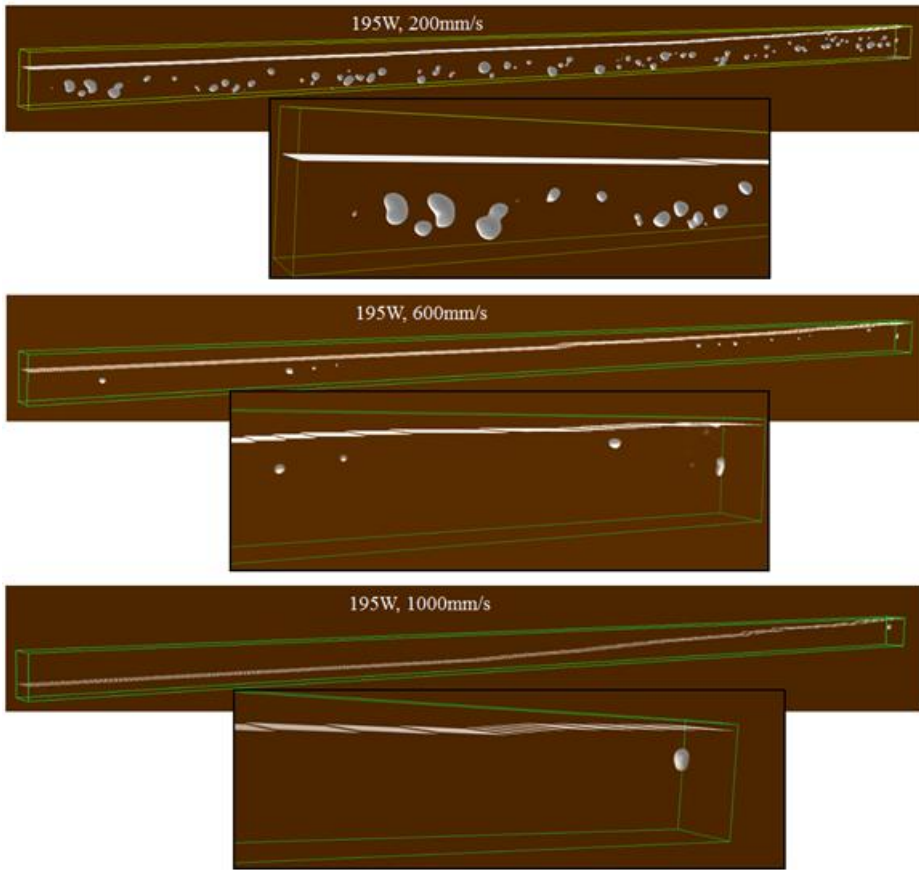
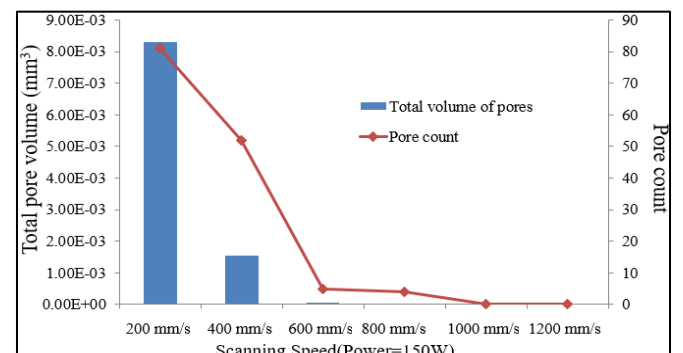
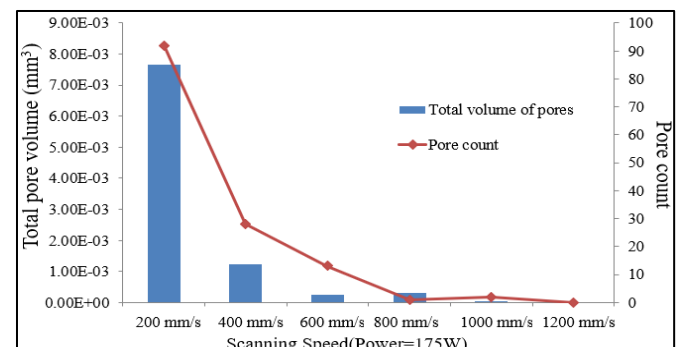
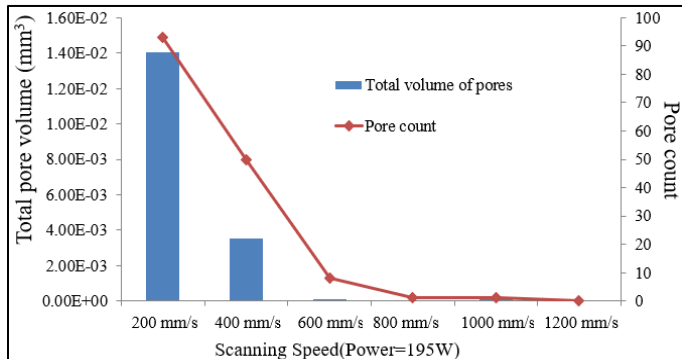


Figure 11: 3D view of pores from single tracks with different speeds.

Individual pore analysis was conducted and the detail information of pore counts and the total pore volume is summarized in Figure 13 for 4 levels of laser power and 6 different scanning speeds. The results show that both the pore volume and the pore count reduce when the scanning speed increases, i.e., from a higher to lower energy density. The maximum porosity was observed for 195 W, 200 mm/s case with energy density of 0.975 J/mm which resulted in 93 pores along single track totaling 0.0141 mm<sup>3</sup> pore volume. Based on the single track morphology and porosity, 195 W and 1200 mm/s (ED=0.1625 J/mm) may be suitable for higher density part production. However, current study has been limited to single track, and the effect of hatch spacing and additive layer should be established to obtain the optimum set of process parameters.



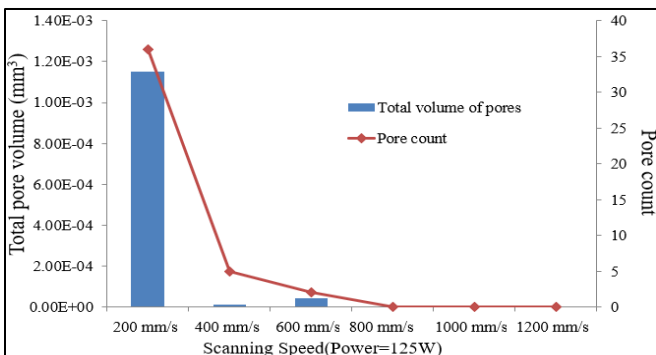


Figure 13: Pore population at different scanning speeds for 195 W, 175 W, 150 W and 125 W.

## CONCLUSIONS

Hollow Ti-6Al-4V cylindrical samples were fabricated using EOS M270 with four single tracks within each specimen. Four power levels: 125 W, 150 W, 175 W and 195 W were used while scanning speeds: 200 mm/s, 400 mm/s, 600 mm/s, 800 mm/s, 1000 mm/s and 1200 mm/s were used to study effect of process parameters on porosity. Porosity analysis on the specimens were performed using a SkyScan 1173 micro-CT scanner. The results clearly show pores resulted from the keyhole phenomenon and following conclusions have been made through this study:

- Porosity is the function of energy density. Within the keyhole region, porosity decreased with decrease in energy density. Among the investigated parameters 195 W and 200 mm/s resulted in maximum number as well as volume of pores.
- Sphericity calculation of pores shows that the pores are near perfect spheres with sphericity greater than 0.8.
- CT scanning results also revealed the track morphology. When the energy density is very low, discontinuous tracks are formed as in 125 W and 1200 mm/s case.

## ACKNOWLEDGEMENTS

This study is supported by NSF (Grant No. 1662662) from the Manufacturing Machine and Equipment program.

## REFERENCES

- [1] Kruth, J.-P., Froyen, L., Van Vaerenbergh, J., Mercelis, P., Rombouts, M., and Lauwers, B., 2004, "Selective laser melting of iron-based powder," *Journal of Materials Processing Technology*, 149(1), pp. 616-622.
- [2] Yadroitsev, I., Krakhmalev, P., Yadroitseva, I., Johansson, S., and Smurov, I., 2013, "Energy input effect on morphology and microstructure of selective laser melting single track from metallic powder," *Journal of Materials Processing Technology*, 213(4), pp. 606-613.
- [3] Rai, R., Elmer, J., Palmer, T., and DebRoy, T., 2007, "Heat transfer and fluid flow during keyhole mode laser welding of tantalum, Ti-6Al-4V, 304L stainless steel and vanadium," *Journal of physics D: Applied physics*, 40(18), p. 5753.
- [4] Panwisawas, C., Qiu, C., Sovani, Y., Brooks, J., Attallah, M., and Basoalto, H., 2015, "On the role of thermal fluid dynamics into the evolution of porosity during selective laser melting," *Scripta Materialia*, 105, pp. 14-17.
- [5] King, W. E., Barth, H. D., Castillo, V. M., Gallegos, G. F., Gibbs, J. W., Hahn, D. E., Kamath, C., and Rubenchik, A. M., 2014, "Observation of keyhole-mode laser melting in laser powder-bed fusion additive manufacturing," *Journal of Materials Processing Technology*, 214(12), pp. 2915-2925.
- [6] Gong, H., Rafi, K., Gu, H., Ram, G. J., Starr, T., and Stucker, B., 2015, "Influence of defects on mechanical properties of Ti-6Al-4 V components produced by selective laser melting and electron beam melting," *Materials & Design*, 86, pp. 545-554.
- [7] Leuders, S., Thöne, M., Riemer, A., Niendorf, T., Tröster, T., Richard, H., and Maier, H., 2013, "On the mechanical behaviour of titanium alloy TiAl6V4 manufactured by selective laser melting: Fatigue resistance and crack growth performance," *International Journal of Fatigue*, 48, pp. 300-307.
- [8] Gong, H., Gu, H., Zeng, K., Dilip, J., Pal, D., Stucker, B., Christiansen, D., Beuth, J., and Lewandowski, J. J., "Melt pool characterization for selective laser melting of Ti-6Al-4V pre-alloyed powder," *Proc. Solid freeform fabrication symposium*, pp. 256-267.
- [9] Aboulkhair, N. T., Everitt, N. M., Ashcroft, I., and Tuck, C., 2014, "Reducing porosity in AlSi10Mg parts processed by selective laser melting," *Additive Manufacturing*, 1, pp. 77-86.
- [10] Weingarten, C., Buchbinder, D., Pirch, N., Meiners, W., Wissenbach, K., and Poprawe, R., 2015, "Formation and reduction of hydrogen porosity during selective laser melting of AlSi10Mg," *Journal of Materials Processing Technology*, 221, pp. 112-120.
- [11] Ponnusamy, P., Masood, S., Ruan, D., Palanisamy, S., and Mohamed, O., "Statistical analysis of porosity of 17-4PH alloy processed by selective laser melting," *Proc. IOP Conference Series: Materials Science and Engineering*, IOP Publishing, p. 012001.
- [12] Holesinger, T. G., Carpenter, J. S., Lienert, T. J., Patterson, B. M., Papin, P. A., Swenson, H., and Cordes, N. L., 2016, "Characterization of an aluminum alloy hemispherical shell fabricated via direct metal laser melting," *JOM*, 68(3), pp. 1000-1011.
- [13] Slotwinski, J. A., Garboczi, E. J., and Hebenstreit, K. M., 2014, "Porosity measurements and analysis for metal additive manufacturing process control," *Journal of research of the National Institute of Standards and Technology*, 119, p. 494.
- [14] Van Bael, S., Kerckhofs, G., Moesen, M., Pyka, G., Schrooten, J., and Kruth, J.-P., 2011, "Micro-CT-based improvement of geometrical and mechanical controllability of selective laser melted Ti6Al4V porous structures," *Materials Science and Engineering: A*, 528(24), pp. 7423-7431.
- [15] Kasperovich, G., Haubrich, J., Gussone, J., and Requena, G., 2016, "Correlation between porosity and processing parameters in TiAl6V4 produced by selective laser melting," *Materials & Design*, 105, pp. 160-170.
- [16] Madison, J. D., Aagesen, L. K., Chan, V. W., and Thornton, K., 2014, "Advancing quantitative description of porosity in autogenous laser-welds of 304L stainless steel," *Integrating Materials and Manufacturing Innovation*, 3(1), p. 11.